Electrochemical properties of doped lithium titanate compounds and their performance in lithium rechargeable batteries

Atef Y. Shenouda [a,*], K.R. Murali [b]

[a] Central Metallurgical Research and Development Institute (CMRDI), Tebbin, P.O. Box 87 Helwan, Cairo, Egypt
[b] Electrochemical Materials Science Division, Central Electrochemical Research Institute (CECRI), Karaikudi 630006, India

Abstract

Several substituted titanates of formula $Li_{4-x}Mg_xTi_{5-x}V_xO_{12}$ ($0 \leq x \leq 1$) were synthesized (and investigated) as anode materials in rechargeable lithium batteries. Five samples labeled as S1–S5 were calcined (fired) at 900 °C for 10 h in air, and slowly cooled to room temperature in a tube furnace. The structural properties of the synthesized products have been investigated by X-ray diffraction (XRD), scanning electron microscope (SEM) and Fourier transmission infrared (FTIR). XRD explained that the crystal structures of all samples were monoclinic while S1 and S3 were hexagonal. The morphology of the crystal of S1 was spherical while the other samples were prismatic in shape. SEM investigations explained that S4 had larger grain size diameter of 15–16 μm in comparison with the other samples. S4 sample had the highest conductivity 2.452×10^{-4} S cm^{-1}. At a voltage plateau located at about 1.55 V (vs. Li $^+$), S4 cell exhibited an initial specific discharge capacity of 198 mAh g^{-1}. The results of cyclic voltammetry for $Li_{4-x}Mg_xTi_{5-x}V_xO_{12}$ showed that the electrochemical reaction was based on Ti^{4+}/Ti^{3+} redox couple at potential range from 1.5 to 1.7 V. There is a pair of reversible redox peaks corresponding to the process of Li$^+$ intercalation and de-intercalation in the Li–Ti–O oxides.
© 2007 Elsevier B.V. All rights reserved.

Keywords: Lithium battery anode; Lithium titanate; Doped lithium titanate-$Li_{4-x}Mg_xTi_{5-x}V_xO_{12}$

1. Introduction

In recent years, lithium secondary batteries have been widely utilized as a power source for mobile electronics; however, modifications are strictly required to apply this type of battery to motor vehicles or energy storage purposes. Even though the excellent cycle characteristics of lithium titanate have been verified for small cells, it exhibits low rate on cycling as active material in large batteries. The reason is due to the extremely small expansion and contraction during the charge and discharge phases of the battery [1]. Lithium titanate spinels, in particular $Li_4Ti_5O_{12}$, has wide interest as insertion electrodes for rechargeable lithium-ion cells and semiconducting materials [2], it was prepared by a solid-state reaction of stoichiometric amounts of TiO_2 and Li_2CO_3 or TiO_2 and LiOH, by heating at 800–1000 °C for 12–24 h [2–10]. The formal potential of Li insertion is 1.55–1.56 V for $Li_4Ti_5O_{12}$ [2–5]. This material accommodates Li with a theoretical capacity of 175 mAh g^{-1} based on the mass of the starting host material. The very fine particulates of lithium titanate (average size of 0.7 mm), prepared by Nakahara et al. [1], showed superior high-rate characteristics, as well as excellent cycle characteristics. A high-capacity maintenance ratio of 99% was achieved at 1 °C and 25 °C after the 100th cycle.

The spherical $Li_4Ti_5O_{12}$ powders with appropriate porosity have been synthesized by spray drying process from rutile type TiO_2 and with polyvinyl butyral (PVB) as pores forming agent [11]. The oxygen atmosphere is very important to the formation of spinel type $Li_4Ti_5O_{12}$ phase with high specific capacity. All specimens showed main discharge platform close to 1.53 V as well as a minor one at about 0.68 V. Overtime heat treatment of the specimens would result in superfluous loss of lithium composition and overgrowth of the particles and therefore reduced their capacity.

The cubic structure of $Li_4Ti_5O_{12}$ can be described in spinel notation $Li_{8a}[Ti_{5/3}Li_{1/3}]_{16d}O_4$, in which 75% of the lithium

* Corresponding author. Tel.: +20 2 5010640; fax: +20 2 5010639.
E-mail addresses: ayshenouda@yahoo.com (A.Y. Shenouda),
muraliramkrish@gmail.com (K.R. Murali).

ions are located on tetrahedral 8a sites, whereas the remaining lithium ions titanium ions reside at the 16 octahedral positions of space group *Fd3m-m* [6]. Lithium is inserted into the spinel structure in a two-phase reaction at a constant potential of approximately 1.5 V versus Li/Li^{2+}. During this reaction the tetrahedral-site lithium ions are cooperatively displaced into neighboring 16c octahedral sites to generate the rock salt phase [Li$_2$]$_{16c}$[Ti$_{5/3}$Li$_{1/3}$]$_{16d}$O$_4$. The [Ti$_{5/3}$Li$_{1/3}$]$_{16d}$O$_4$ spinel framework is extremely robust and provides a three-dimensional interstitial space of face-shared 8a tetrahedral and 16c octahedra for lithium-ion transport through the crystalline bulk structure. Although the voltage of Li$^+$/Li$_4$Ti$_5$O$_{12}$ cell is too low for Li$_4$Ti$_5$O$_{12}$ to be an attractive positive electrode, it can be coupled as a negative electrode with a LiCoO$_2$ or LiMn$_2$O$_4$ positive electrode to yield 2.5 V lithium-ion cells with significantly improved safety features over conventional high voltage (3.5 V) Li$_y$C$_6$/Li$_{1-y}$CoO$_2$ cells, albeit at the expense of cell voltage and energy density.

Among the critical requirements of lithium insertion electrode is that the electrode should have both good electronic conductivity and good Li$^+$ ion conductivity in order to achieve fast reaction rates (high power) for the lithium cell [12]. Because of the insulation properties of Li$_4$Ti$_5$O$_{12}$ spinel phase, Li$_7$Ti$_5$O$_{12}$ with mixed Ti^{4+}/Ti^{3+} valence is produced in order to induce excellent electronic conductivity at the particle surface of the spinel electrode and thus allowing the rapid transfer of electrons to external circuit. However, it is anticipated that the opposite is true when lithium is extracted from Li$_7$Ti$_5$O$_{12}$ electrodes, i.e. the insulating Li$_4$Ti$_5$O$_{12}$ spinel phase is formed on the particle surface, thereby limiting the rate at which electron transfer to the external circuit can occur.

Thackeray [13] reported that it is possible to synthesize Li–Ti–O spinel electrodes with mixed Ti^{4+}/Ti^{3+} valence and to enhance the electronic conductivity of these electrodes by varying the Li:Ti ratio along the stoichiometric Li$_4$Ti$_5$O$_{12}$–LiTi$_2$O$_4$ spinel tie-line of the Li–Ti–O phase diagram. Such a solid solution can be represented by the general formula Li$_{1+\delta}$Ti$_{2-\delta}$O$_4$ for the range ($0 \leq \delta \leq 0.33$). At $\delta = 0$, the spinel LiTi$_2$O$_4$ has an average Ti valence of 3.5; this compound is metallic and becomes superconducting at 11 K [14]. However, it is more difficult to synthesize compounds within the Li$_{1+\delta}$Ti$_{2-\delta}$O$_4$ spinel system compared to the manganese Li$_{1+\delta}$Mn$_{2-\delta}$O$_4$ system because of the relative instability of Ti^{3+}.

Chen et al. [15] studied the electrochemical behavior of Mg-doped spinel Li$_4$Ti$_5$O$_{12}$ and reported that the substitution of divalent Mg ions for monovalent Li ions in the structure necessitates that the difference in charge must be compensated by a reduction of an equivalent number of Ti cations from Ti^{4+} to Ti^{3+}. The substitution increases the conductivity of the [Ti$_{5/3}$Li$_{1/3}$]O$_4$ spinel framework from Li$_4$Ti$_5$O$_{12}$ to LiMgTi$_5$O$_{12}$, in which the average titanium oxidation state is 3.8.

The spinel Li$_4$Ti$_5$O$_{12}$ showed a voltage plateau at 1.55 V versus Li/Li$^+$ and intercalated reversibly 3Li atom per formula unit giving 175 Ah kg^{-1} at the afore-mentioned voltage [3]. Li$_4$Ti$_5$O$_{12}$ can also be used as negative electrode of 2 V in

lithium-ion batteries as it showed good cycling performance and the change in its cubic unit cell volume is only less than 0.2% during charge/discharge processes.

Ariyoshi et al. [16] examined the combination between Li$_4$Ti$_5$O$_{12}$ (*Fd3m-m*; $a = 8.36$ Å) and LiNi$_{0.5}$Mn$_{1.5}$O$_4$ (*Fd3m-m*; $a = 8.17$ Å) with emphasis on rate-capacity and cycle life. This cell showed a quite flat operating voltage of 3.2 V versus Li$^+$ with excellent cycleability. Accelerated cycle tests indicated that 83% of the initial capacity was delivered and stored even after 1100 cycles. Although the calculated energy density of a Li[Li$_{1/3}$ Ti$_{5/3}$]O$_4$/Li[Ni$_{1/2}$ Mn$_{3/2}$]O$_4$ cell was about 250 Wh kg^{-1}or 1000 Wh dm^{-3} based on the active material weight or volume, the 3 V lithium-ion battery exhibited positive characteristic features, such as flatness in operating voltage, high-rate capacity and cycle life.

Ramsdellite titanates phases (composed of distorted MO$_6$ octahedra; where M is Ti atom) in the system Li$_{1+x}$Ti$_{2-2x}$O$_4$ have been studied by Irvine et al. [17]. These phases had good electrochemical insertion behavior and appeared to be potential Li-ion negative materials, similar to the spinel Li$_4$Ti$_5$O$_{12}$. The ramsdellite phases showed a similar reversible peak at just less than 1.5 V versus Li/Li$^+$.

The aim of the present work is to improve the electrochemical behavior of lithium titanate as anodic material by doping with some ratios of magnesium and vanadium. To the best of the Authorsǐ knowledge, not too much work has been reported using the above-mentioned two elements with lithium titanate.

2. Experimental

2.1. Sample preparation and characterization

The starting reagents, Li$_2$CO$_3$ (S.D. Fine-Chem. Ltd., 99%), MgCO$_3$ (Aldrich, 99%), TiO$_2$ (anatase, BDH, 99.9%) and NH$_4$VO$_3$ (CDH, 99%), were dried overnight prior to use and then weighed with stoichiometric ratios in order to get Li$_{4-x}$Mg$_x$Ti$_{5-x}$V$_x$O$_{12}$; where ($0 \leq x \leq 1$). Five samples labeled as S1–S5 were prepared taking: $x = 0$, 0.25, 0.5, 0.75 and 1, respectively. Powder of the precursor materials were mixed and ground in a mortar with some drops of acetone. The powder mixture of samples was dried in an oven at 150 °C for 1/2 h and finally fired at 900 °C for 10 h in air. Samples S1–S5 were slowly cooled to room temperature (RT). After that, the samples were ground and fired again at 900 °C for 6 h and slowly cooled to RT.

The materials were characterized by X-ray diffraction (XRD) using Philips Powder diffractometer with Cu Kα radiation. Scanning electron microscopy (SEM) (Hitachi S3000H) was used to investigate the morphology of the crystals. Infrared absorption spectra were recorded using a Bruker IFS113 vacuum FTIR interferometer. Samples were ground to fine powders, mixed approximately 1:300 with KBr, and vacuum pressed into translucent disks. The measurements were carried out in the far-infrared region (400–4000 cm^{-1}). Elemental analysis was performed by X-ray fluorescence (Philips PW 1410 Spectrometer) and Inductive coupled plasma (ICP Perkin-Elmer Optima 2000 DV).

2.2. Electrochemical measurements

Impedance spectroscopy was carried out in the frequency range from 1 MHz to 10 mHz using IM6 Zaher frequency response analyzer. The AC amplitude was 50 mV. The prepared samples were pressed into pellets at 1 tonnes cm^{-2} and coated with silver paste that acts as current collector. The pellets diameters were in range of 12.5–13.1 mm and also their thickness varied between 3 and 3.3 mm. Cycle life and cyclic voltammetric measurements (CV) were performed by using a coin cells 20 mm diameter comprising the active material electrode (working electrode) and lithium metal foil (Merck, Darmstadt, Germany) as both counter and reference electrode.

Li$_{4-x}$Mg$_x$Ti$_{5-x}$V$_x$O$_{12}$ synthesized powders, black carbon and PTFE were mixed in a weight ratio of 85:10:5, respectively to fabricate composite working electrode in *n*-methyl pyrrolidone (NMP) solvent to form homogeneous slurry. The slurry was then spread onto an Al foil sheet. The coated sheet was dried in an oven at 120 °C for 12 h. The sheet was then pressed at a pressure of 1500 kg cm^{-2}. After that it was cut into circular electrodes of 14 mm diameter. The active material loading was about 2–3 mg for each individual electrode. The cells were assembled in an argon filled glove box (Mbraun, Unilab, Germany). The separator was made up of a circular porous polypropylene soaked in a 1M LiClO$_4$ dissolved in a propylene carbonate (PC) (Fluka, 99%). All potentials were recorded versus Li/Li$^+$ electrode. The galvanostatic charging–discharging measurements were carried using current densities 0.20 and 0.15 mA cm^{-2}, respectively. CV measurements were carried out using scan rate 0.1 mV s^{-1} and the potential windows were 1 and 3 V versus Li/Li$^+$ electrode. CV measurements were carried out with a Potentiostat, Auto-Lab. The test cells incorporating the above components were fabricated inside a glove box filled with dry argon.

3. Results and discussion

3.1. IR analysis

Fig. 1a shows the FTIR spectra of the samples prepared by slow cooling between 400 and 900 cm^{-1}. There are broad peaks in the range of 625–630 cm^{-1}. This type of peaks represents symmetric stretching vibration of Ti–O bond [18,19]. As shown in Fig. 1b, S2–S5 samples have small peaks at 960, 980, 990 and 1010 cm^{-1}, respectively. These peaks correspond to stretching vibration V=O bond [20,21]. So, the bond lengths of V=O decrease with increase of vanadium ratio. Therefore, S4 and S5 have V=O bond type similar to the same one in V$_2$O$_5$ (995–1020 cm^{-1}) [21]. Third type of peaks appears at 1040, 1060, 1090 and 1100 cm^{-1} for S2–S5, respectively. It is observed that increasing the ratios of V and Mg increase the wave numbers of these peaks. Also, the absorption intensities of peaks as illustrated in Fig. 1 increase from S1 to S4 and after that decrease with S5. This behavior reflexes the higher crystallinity of S4 than the other samples as observed in the SEM investigations [19]. Fig. 2a shows Raman spectra of S1. There are main three absorption peaks at 250, 440 and 680 cm^{-1} for σTiO, ν_{asy}TiO and ν_{sy}TiO, respectively [22]. Similar peaks are
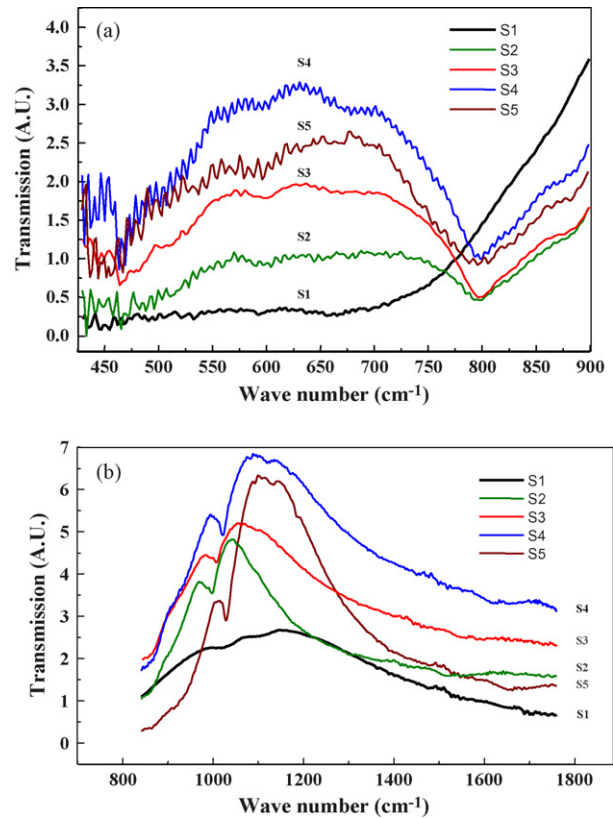
Fig. 1. FTIR spectra of the Li$_{4-x}$Mg$_x$Ti$_{5-x}$V$_x$O$_{12}$; x = 0, 0.25, 0.5, 0.75 and 1 for S1–S5, respectively.

observed for S4 beside the V–O–V asymmetric stretch as shown in Fig. 2b. In general, it is noticed that the vibration modes of these peaks correspond to octahedral group MO$_6$ lattice located in the molecular structure [18].

3.2. Structural characterization and morphological investigation

The crystal structure and phase composition of the five specimens were investigated by XRD as shown in Fig. 3. Table 1 explained the unit cell parameters of the samples using software analysis with the XRD patterns. S1 and S3 have hexagonal crystal structure. The other samples are monoclinic. The XRD pattern of S1, Li–Ti–O ternary phase prepared from Li$_2$CO$_3$ and TiO$_2$ (anatase) does not contain a peak at $2\theta = 25°$ characteristic to TiO$_2$. This indicates that TiO$_2$ has been fully consumed in the solid-state reaction [23]. The presence of weak [2 2 0] peaks at $2\theta \sim 30.18°$ as observed in S2–S5 samples are for Li$_3$MgTi$_5$O$_{12}$ as reported by some authors [15]. Also, *c/a* value and cell volume of S4 is higher in comparison with the other samples. So, the insertion and de-insertion of Li ions are easier for this sample [24].

Fig. 4 shows the morphological changes in the crystals shape. It is apparent that S1 has spherical shape. The other samples consist of prismatic particles. The average crystal size increases from S1 to S4, respectively and after that decreases towards S5. The average grain size diameter of the crystals is illustrated in Fig. 5. S1 has average grain size of ~1.5 μm while

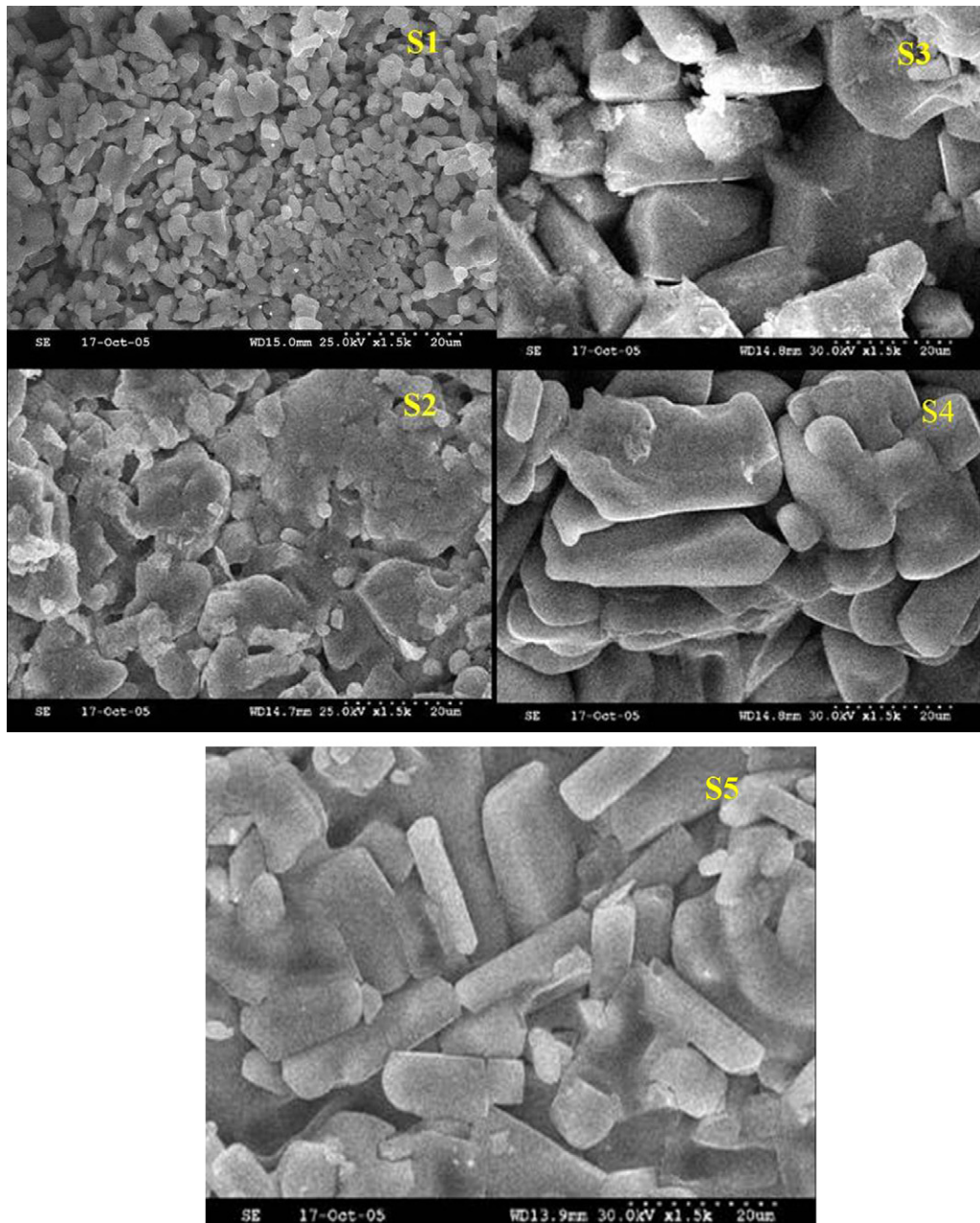Fig. 2. Raman spectra of (a) S1 ($Li_4Ti_5O_{12}$) and (b) S4 ($Li_{3.25}Mg_{0.75}$ $V_{0.75}Ti_{4.75}O_{12}$).

Fig. 3. X-ray diffraction patterns of $Li_{4-x}Mg_xTi_{5-x}V_xO_{12}$ prepared at 900 °C: (a) $x = 0$, 0.25 and 0.5 and (b) $x = 0.75$ and 1.

S4 has larger grain size diameter of 15–16 μm than the other samples.

3.3. Electrochemical measurements

Results from impedance spectra measurements for the prepared samples materials are shown in Fig. 6. The impedance spectra are composed of one semicircle at higher frequencies followed by linear part at lower frequency end. The bulk resistivities of the sample pellets (r_b) have the obtained values: 6.841×10^5, 3.665×10^4, 2.108×10^4, 4.065×10^3 and 1.90×10^4 Ω cm for S1–S5, respectively. It is observed that S4 has the lowest resistivity value and consequently, it has higher conductivity: 2.46×10^{-4} S cm^{-1}.

The impedance spectra of the cells showed an intercept at high frequency, followed by a semicircle in the high-middle frequency region, and a straight line in the low frequency region Fig. 7. The intercept impedance on the Z_{real} axis represents the ohmic resistance, which consists of the resistance of the electrolyte and electrode. The high-frequency region of the semicircle represents the migration of the Li$^+$ ions at the electrode/electrolyte interface through the solid electrolyte interface (SEI) layer, whereas the middle frequency range of the semicircle corresponds to the charge-transfer process. The low frequency region of the straight line is attributed to the diffusion of the lithium ions into the bulk of the electrode material or so-called Warburg diffusion. The cells resistances with S4 and S5 had lower values of about 80 Ω. Therefore, higher conductivity of S4 could be attributed to the addition of Mg and V ions [25].

Table 1
Unit cell parameters of the samples

Sample	unit cell parameters (Å)			c/a ratio	Cell angle, β (°)	Cell volume (Å^3)
	a	b	c			
S1	11.054	11.054	10.415	0.9421	Hexagonal	1102.1
S2	8.6959	10.1130	7.9404	0.7981	90.374	610.32
S3	9.603	9.603	9.605	1.0002	Hexagonal	885.7501
S4	12.501	6.324	14.808	1.1845	93.57	1170.66
S5	10.019	9.908	11.361	1.1339	96.61	1125.6

Fig. 4. SEM of $Li_{4-x}Mg_xV_xTi_{5-x}O_{12}$ compounds; $0 \leq x \leq 1$.
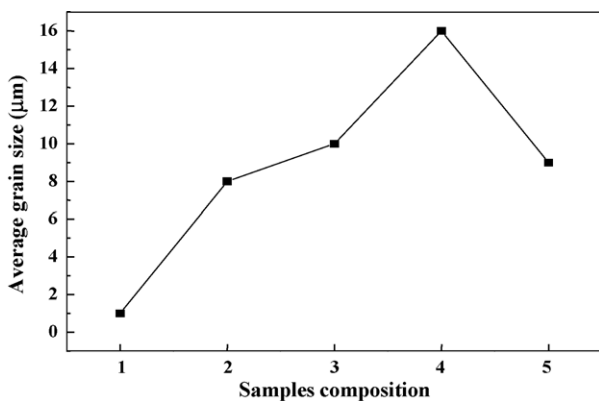

Fig. 5. Average grain size of samples $Li_{4-x}Mg_xV_xTi_{5-x}O_{12}$; $0 \leq x \leq 1$.

AC impedance spectra were fitted using an equivalent circuit, which is shown in Fig. 8. A constant phase element CPE was placed to represent the double layer capacitance and passivation film capacitance. The parameters of the equivalent circuit are shown in Table 2. It is revealed that the exchange current densities ($i^0 = RT/nFR_{ct}$) of S4 and S5 cells are higher than the other ones. The resistance of the combination of the electrolyte and electrode (R_e) is almost similar for the different prepared electrodes. This is because the electrodes were prepared by adding a conductive carbon black agent, which induces good conductivity of the electrode. The doped electrode with Mg and V exhibited much lower charge-transfer resistance than that of the bare $Li_4Ti_5O_{12}$, indicating that the doping by these two elements increased significantly the electrical conductivity of $Li_4Ti_5O_{12}$.
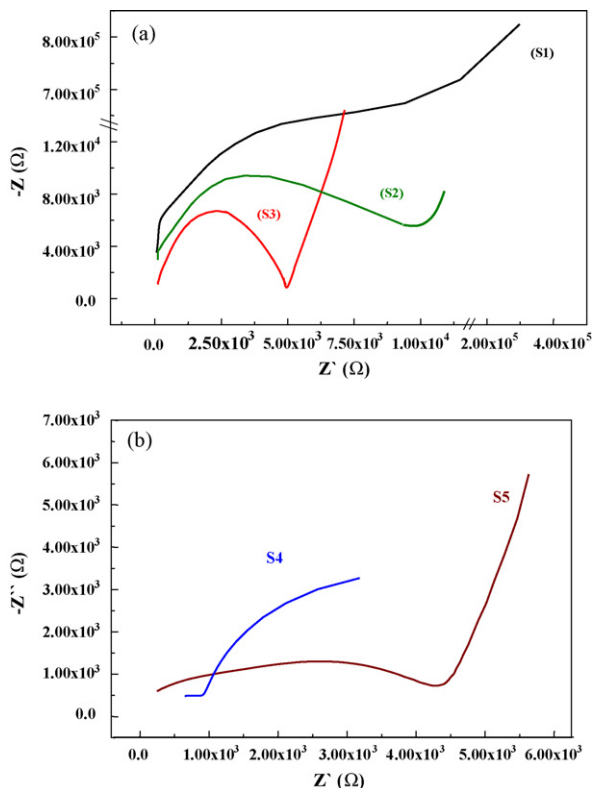
Fig. 6. EIS of (a) S4 and (b) S5 material pellets.

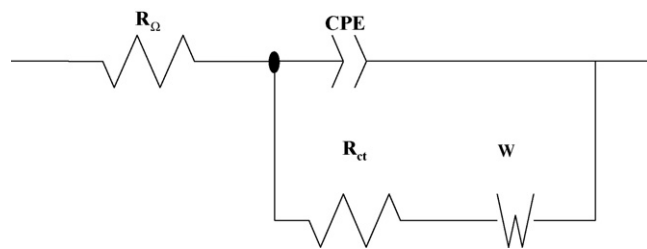Fig. 8. Equivalent circuit used for fitting the experimental AC impedance data.

Table 2
Impedance parameters of the S1–S5 cells

Sample	R_e (Ω)	R_{ct} (Ω)	i^0 (mA cm^{-2})
S1	28	10^4	2.56×10^{-3}
S2	25	10^4	2.56×10^{-3}
S3	22	2740	9.36×10^{-3}
S4	18.97	81	0.316
S5	25.83	81	0.316

Therefore, the Mg and V doping can facilitate the charge-transfer reaction of $Li_4Ti_5O_{12}$ electrodes.

The 1st cyclic voltammograms are recorded in Fig. 9. The curves show one cathodic peak located at ∼1.5 (vs. Li$^+$) corresponding to the voltage flat of the first discharge process at the same voltage. This is the process of Li insertion in $Li_4Ti_5O_{12}$. There are also other anodic peaks at 1.7 V (vs. Li$^+$) correspond to the voltage flat of the first charge process. This is the process of Li$^+$ ion de-intercalation from $Li_4Ti_5O_{12}$. It is typical behavior for two-phase reaction during Li$^+$ ion extraction and insertion process. The corresponding electrochemical processes are:

$$Li_4Ti_5O_{12} + 3Li^+ + 3e^- \rightarrow Li_7Ti_5O_{12} \quad E = 1.5\,V \quad (1)$$
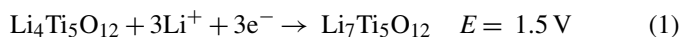
The electrochemical reaction based on Ti^{4+}/Ti^{3+} redox couple is a reversible redox reaction. Similar results are reported by some authors [18,26,27].

Fig. 10 shows the initial specific charge and discharge capacities of cells prepared using samples S1–S5 as cathode and lithium metal as anode in the voltage range between 1 and 3 V versus Li$^+$. During the discharge, the voltage drops quickly down
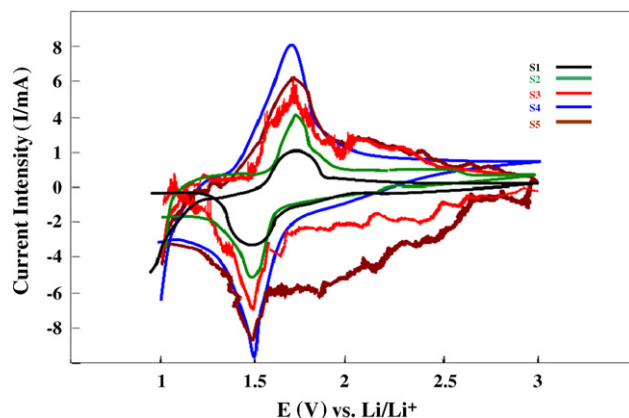

Fig. 7. EIS of S1–S5 cells.

Fig. 9. Cyclic voltammograms of S1–S5 cell, scan rate; 10^{-4} V s^{-1}.
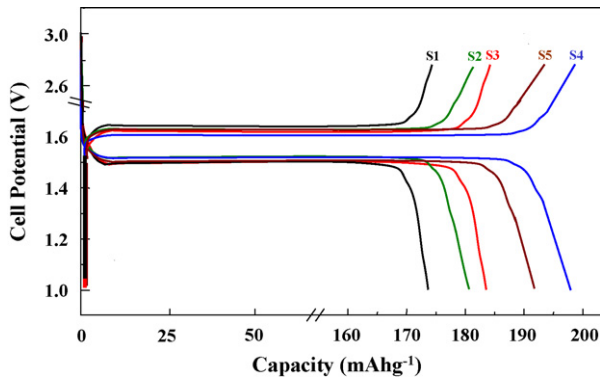
Fig. 10. First specific charge and discharge capacity of $Li_{4-x}Mg_xTi_{5-x}V_xO_{12}$ samples.

4. Conclusion

Anode materials $Li_{4-x}Mg_xTi_{5-x}V_xO_{12}$; where $(0 \leq x \leq 1)$ for lithium batteries have been easily synthesized by solid-state reaction. The addition of Mg and V ions improve the conductivity of the material as observed in S4 ($Li_{3.25}Mg_{0.75}Ti_{4.25}V_{0.25}O_{12}$). The higher value of *c/a* parameter in S4 facilitates the insertion and de-insertion of the Li ions in the crystal lattice. S4 cell showed higher electrical conductivity, specific discharge capacity and cycle life than the other cells.

Acknowledgment

to below 2 V and decreases as the reaction proceeds until the voltage reaches ~1.55 V (vs. Li). After which the voltage profile has an extremely flat operating voltage at about 1.55 V. A very flat charge curve at about 1.6 V (vs. Li) can be observed. This suggests a two-phase reaction based on the Ti^{4+}/Ti^{3+} redox couple [4,18,26]. S4 cell delivered an initial specific discharge capacity 198 mAh g^{-1}, while the other samples delivered lower values. The obtained specific discharge capacity of S4 cell is higher than the ones reported by Chen et al. [15] for $Li_4Ti_5O_{12}$ and $Li_3MgTi_5O_{12}$ (175 and 169 mAh g^{-1}, respectively). They explained that the lower capacity delivered by $Li_3MgTi_5O_{12}$ electrodes was due to the higher concentrations of Mg^{2+}. Also, the unit cell parameters of S1 and S4 as shown in Table 1 were greater than that reported of the cubic spinel crystal structure $Li_4Ti_5O_{12}$ (8.358–8.364 Å) [15,22,26,28]. Therefore, the insertion and de-insertion of Li^+ ions have more mobility in S1 and S4 rather than the cubic spinel one. Thus, increasing of the Li^+ ions mobility improves the specific discharge capacity.

Cycling performance of the samples is shown in Fig. 11. The first specific discharge capacity of S4 was 198 and 187 mAh g^{-1} after 25 cycles but there was a stability in the capacity for the other cycles. The other samples had the same behavior but with lower capacities. Approximately, these samples are stable in their capacities after 60 cycles.
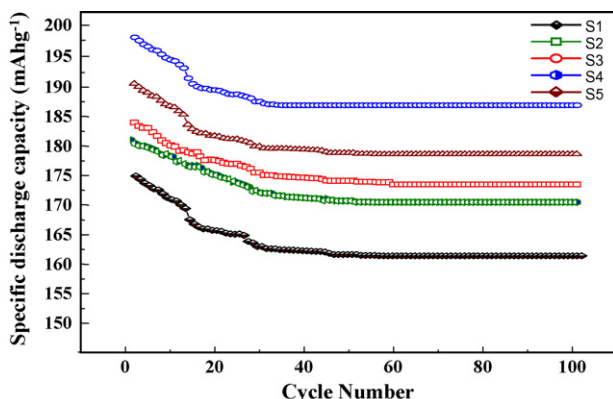

Fig. 11. Cycling performance of Li/$Li_{4-x}Mg_xTi_{5-x}V_xO_{12}$; $0 \leq x \leq 1$ cells.

References

[1] K. Nakahara, R. Nakajima, T. Matsushima, H. Majima, J. Power Sources 117 (2003) 131–136.

[2] T. Brousse, P. Fragnaud, R. Marchand, D.M. Schleich, O. Bohnke, K. West, J. Power Sources 68 (1997) 412–415.

[3] E. Ferg, R.J. Gummov, A. de Kock, M.M. Thackeray, J. Electrochem. Soc. 141 (1994) L147.

[4] T. Ohzuku, A. Ueda, N. Yamamoto, J. Electrochem. Soc. 142 (1995) 1431.

[5] M.R. Harrison, P.P. Edwards, J.B. Goodenough, Philos. Mag. B 52 (1985) 679.

[6] S.I. Pyun, S.W. Kim, H.C. Shin, J. Power Sources 81–82 (1999) 248.

[7] S. Scharner, W. Weppner, P. Schmid Beurmann, J. Electrochem. Soc. 146 (1999) 857.

[8] K. Zaghib, M. Simoneau, M. Armand, M. Gauthier, J. Power Sources 81–82 (1999) 300.

[9] K. Zaghib, M. Simoneau, M. Armand, M. Gauthier, J. Electrochem. Soc. 145 (1998) 3135.

[10] S. Takai, M. Kamata, S. Fujine, K. Yoneda, K. Kanda, T. Esaka, Solid State Ionics 123 (1999) 165.

[11] Z. Wen, Z. Gua, S. Huang, J. Yang, Z. Lin, O. Yamamoto, J. Power Sources 146 (2005) 670–673.

[12] A.N. Jansen, A.J. Kahaian, K.D. Kepler, P.A. Nelson, K. Amine, D.W. Dees, D.R. Vissers, M.M. Thackeray, J. Power Sources 81–82 (1999) 902.

[13] M.M. Thackeray, Prog. Solid State Chem. 25 (1997) 1.

[14] D.C. Johnston, J. Low Temp. Phys. 25 (1976) 145.

[15] C.H. Chen, J.T. Vaughey, A.N. Jansen, D.W. Dees, A.J. Kahaian, T. Goacher, M.M. Thackeray, J. Elecrochem. Soc. 148 (2001) A102–A104.

[16] K. Ariyoshi, S. Yamamoto, T. Ohzuku, J. Power Sources 119–121 (2003) 959–963.

[17] R. Gover, K.B. Tolchard, J.R. Tukamoto, H. Murai, T. John, T.S. Irvine, J. Electrochem. Soc. 146 (1999) 4348.

[18] Y. Hao, Q. Lai, Z. Xu, X. Liu, X. Ji, Solid State Ionics 176 (2005) 1201–1206.

[19] G.C. Allen, M. Paul, Spectroscopy 49 (1995) 451.

[20] A.Y. Shenouda, Electrochim. Acta 51 (2006) 5973–5981.

[21] H.N. Ng, C. Calvo, Can. J. Chem. 50 (1972) 3619.

[22] Y.J. Hao, Q. Yu Lai, D. Liu, Z. Xu, X.Y. Ji, Mater. Chem. Phys. 94 (2005) 382–387.

[23] D. Peramunage, K.M. Abraham, J. Electrochem. Soc. 145 (1998) 2609.

[24] B.L. Cushing, S.H. Kang, J.B. Goodenough, Int. J. Inorg. Mater. 3 (2001) 875.

[25] T.H. Teng, M. Yang, S. Wu, Y.-P. Chiang, Solid State Commun. 142 (2007) 389–392.

[26] Y. Hao, Q. Yu Lai, J.Z. Lu, H. Li Wang, Y.D. Chen, X.Y. Ji, J. Power Sources 158 (2006) 1358–1364.

[27] A. Du Pasquier, A. Laforgue, P. Simon, J. Power Sources 125 (2004) 95.

[28] C.L. Wang, Y.C. Liao, F.C. Hsu, N.H. Tai, M.K. Wu, Electrochem. J. Soc. 152 (2005) A653–A657.